

# Hybrid 3D/Inkjet-Printed Organic Neuromorphic Transistors

Tanyaradzwa N. Mangoma,\* Shunsuke Yamamoto, George G. Malliaras, and Ronan Daly\*

Organic electrochemical transistors (OECTs) are proving essential in bioelectronics and printed electronics applications, with their simple structure, ease of tunability, biocompatibility, and suitability for different routes to fabrication. OECTs are also being explored as neuromorphic devices, where they emulate characteristics of biological neural networks through co-location of information storage and processing on the same unit, overcoming the von Neumann performance bottleneck. To achieve the long-term vision of translating to inexpensive, low-power computational devices, fabrication needs to be feasible with adaptable, scalable digital techniques. Here, a hybrid direct-write additive manufacturing approach to fabricating OECTs is shown. 3D printing of commercially available printing filament is combined to deliver conducting and insulating layers, with inkjet printing of semiconducting thin films to create OECTs. These printed OECTs show depletion mode operation paired-pulse depression behavior and evidence of adaptation to support their translation to neuromorphic devices. These results show that a hybrid of accessible and design-flexible AM techniques can be used to rapidly fabricate devices that exhibit good OECT and neuromorphic performances.

components.<sup>[1]</sup> They consist of an organic semiconductor thin film patterned between two electrodes, the source and the drain. The semiconductor thin film is in contact with an electrolyte in which a gate electrode is immersed. With application of a gate voltage ( $V_G$ ), ions from the electrolyte enter the semiconductor, changing its doping state and conductivity, which in turn changes the current that flows between the source and the drain (drain current,  $I_D$ ).<sup>[2]</sup> This volumetric doping mechanism is highly efficient, leading to large changes in  $I_D$  for small changes in  $V_G$ . As a result, OECTs show very high transconductance ( $g_m = \partial I_D / \partial V_G$ ), which is a parameter that governs signal amplification.<sup>[3]</sup> The response time, however, for OECTs is typically quite slow, as ions must penetrate through the entire film.<sup>[4]</sup> This combination of characteristics makes OECTs suitable for applications in bioelectronics and some areas of large-area electronics, most notably printable electronics.<sup>[1,5,6]</sup>

## 1. Introduction

Organic electrochemical transistors (OECTs) are receiving a great deal of attention owing to their simple structure, tunability, biocompatibility, and the ease of deposition of organic

electronics, most notably printable electronics.<sup>[1,5,6]</sup>


Recently, the characteristics of OECTs have also led to them being explored as neuromorphic devices.<sup>[7,8]</sup> These are devices that emulate processing functions observed in biological neural networks and are being developed for computing systems that consume less power and overcome the von Neumann performance bottleneck.<sup>[9]</sup> An identifying characteristic of biological neural networks is that storage and processing of information is co-located on the same unit.<sup>[10]</sup> One manifestation of this is Hebbian learning, according to which synaptic connections become more efficient upon repeated stimulation of the post-synaptic by the pre-synaptic neuron (neurons that fire together wire together).<sup>[11]</sup> This property can be captured in OECTs, when repeated voltage pulses at the gate (the equivalent of the pre-synaptic input) lead to ion accumulation in the semiconductor, thereby have a cumulative effect on the drain current (the post-synaptic output). Leveraging this property, processing functions including synaptic plasticity, orientational selectivity, and homeoplasticity have been demonstrated with OECTs.<sup>[7,12,13]</sup>

Photolithography is still by far the most commonly reported approach for fabricating OECTs.<sup>[3,14–17]</sup> However, the simple structure of OECTs and the ease of formulation of organic materials into different material formats have enabled fabrication using a variety of manufacturing techniques, such as screen printing, spin coating, inkjet printing, and gel extrusion.<sup>[18–22]</sup> Photolithography is highly efficient, with excellent yields, high achievable resolution, and scalability, but in research and also low-volume, late-stage manufacturing, there is often a greater

T. N. Mangoma, Dr. R. Daly  
Institute for Manufacturing  
University of Cambridge  
17 Charles Babbage Road, Cambridge CB3 0FS, UK  
E-mail: tm617@cam.ac.uk; rd439@cam.ac.uk

Dr. S. Yamamoto,<sup>[†]</sup> Prof. G. G. Malliaras  
Electrical Engineering Division  
Department of Engineering  
University of Cambridge  
9 JJ Thomson Avenue, Cambridge CB3 0FA, UK

Dr. S. Yamamoto  
Institute of Multidisciplinary Research for Advanced Materials  
Tohoku University  
2-1-1 Katahira, Sendai 9808577, Japan

 The ORCID identification number(s) for the author(s) of this article can be found under <https://doi.org/10.1002/admt.202000798>.

© 2020 The Authors. Advanced Materials Technologies published by Wiley-VCH GmbH. This is an open access article under the terms of the Creative Commons Attribution License, which permits use, distribution and reproduction in any medium, provided the original work is properly cited.

<sup>[†]</sup>Present address: Graduate School of Engineering, Tohoku University, 6-6-11 Aramaki Aza Aoba, Aoba-ku, Sendai 980-8579, Japan

DOI: 10.1002/admt.202000798

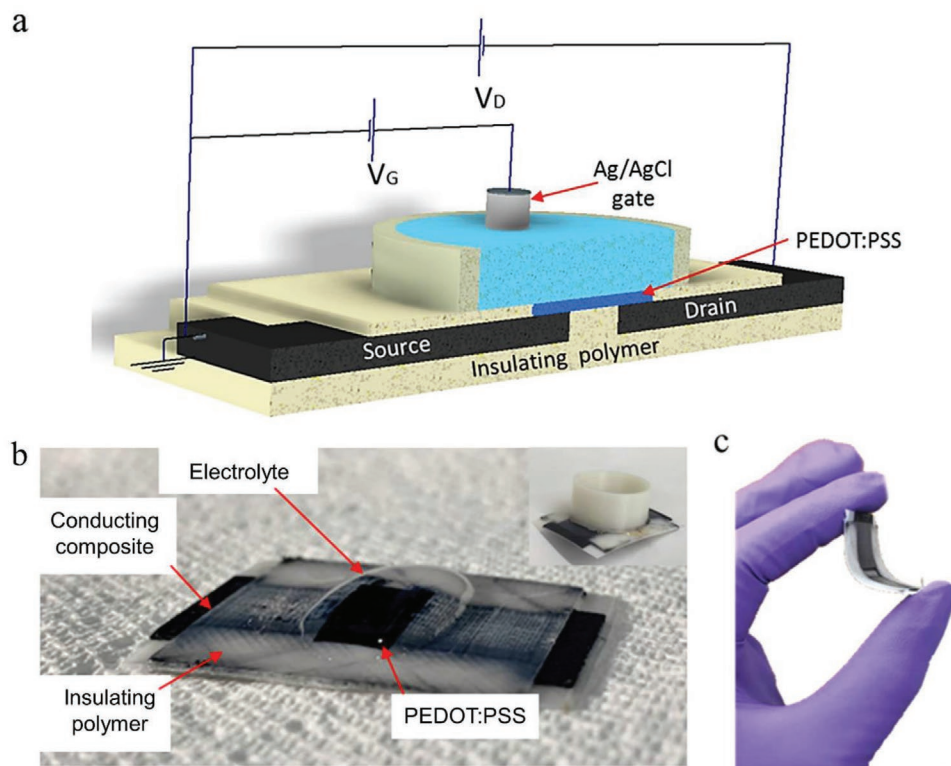


**Figure 1.** An additively manufactured OEET device. a) Schematic of the designed OEET. b) Images of the 3D and inkjet-printed device showing the 3D printed conducting electrodes and insulating layer, and the region of the inkjet-printed PEDOT:PSS. The electrolyte is also indicated. An inset shows device with a well attached for more controlled electrolyte containment, c) illustrating device flexibility.

need for rapid design change and digitally enabled direct-write techniques.<sup>[23]</sup> In this study, we propose an accessible, hybrid direct-write additive manufacturing approach to fabricating OEETs. We prepare electrodes and dielectric layers using standard inexpensive 3D printers, specifically fused deposition modeling (FDM) and commercially available materials. The semiconductor thin film is added by inkjet printing, a more precise deposition tool. This combination enables fabrication of neuromorphic OEETs that operate in the depletion regime and exhibit the neuromorphic processing functions of paired-pulse depression and adaptation.

## 2. Results and Discussion

### 2.1. Overview of Device Structure

**Figure 1** shows an illustration and images of the additively manufactured OEET, with details of the hybrid additive fabrication technique outlined in the Experimental Section. An initial base layer of insulating thermoplastic co-polyester (TPC) is deposited by FDM. A conducting carbon-filled polylactide resin composite(c-PLA) is then used to create the source and drain electrodes on top of the insulating layer, again by FDM. Inkjet printing is used to deposit a commercially available doped semiconductor, PEDOT:PSS, to behave as the active layer, bridging the c-PLA source and drain electrodes. Finally, TPC is further deposited by FDM to first insulate the electrodes and second, to create a well to contain the electrolyte (phosphate-buffered

saline (PBS)). Finally, an Ag/AgCl pellet is used as the gate electrode and the device is biased as shown in **Figure 1a**. **Figure 1b,c** shows images of a device before the well is deposited (a device with a well is shown in the inset of **Figure 1b**). The devices are 35 mm in length. An optical micrograph of a cross section of the channel region, including electrodes and insulating layers, is presented in **Figure S1**, Supporting Information.

### 2.2. OEET Characterization

Twelve devices were fabricated and tested for the architecture shown in **Figure 1**. **Figure 2** shows transistor characteristics from one of the printed OEET devices that were used to carry out all the measurements in this publication. These findings are representative of typical characteristics seen from all printed devices. The transient to steady state behavior of the gate ( $I_G$ ) and drain currents ( $I_D$ ) to a gate pulse are shown in **Figure 2a**. The device was biased to a drain voltage ( $V_D$ ) of  $-900$  mV, and a gate pulse of 800 mV was applied for 200 s. The gate current appears only when the transistor is switched on or off. This is consistent with the fact that the gate current is caused by ions injected from the electrolyte into the semiconductor and vice versa. The drain current, on the other hand, shows a significant decrease that persists for the duration of the gate pulse. This is consistent with the fact that PEDOT:PSS is a p-type organic semiconductor that gets de-doped by cations upon the application of a negative gate voltage. It should be noted that the spikes seen in the drain

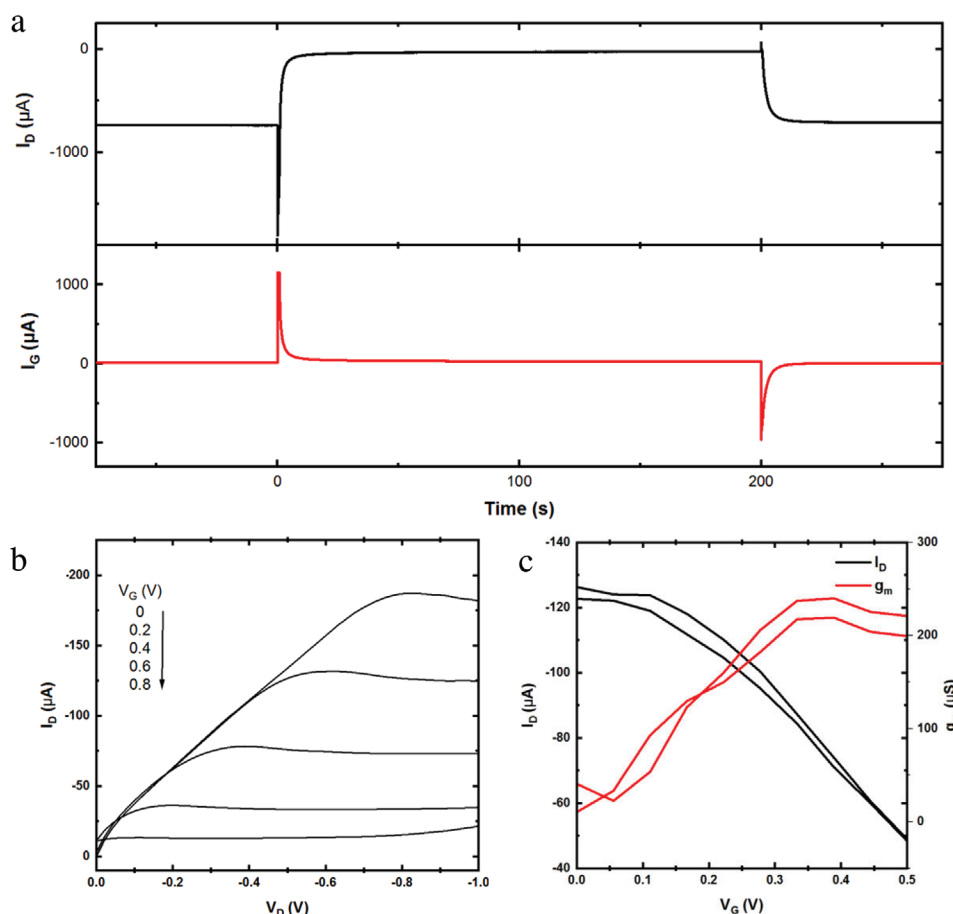


**Figure 2.** Transistor characteristics of the device. a) Response to a single gate pulse. Amplification in  $I_D$  can be seen. A spike and recovery characteristic can be seen around  $T = 0$ , indicating neuromorphic behavior in the device. b,c) Output and transfer characteristics obtained from the device. Results verify that hybrid inkjet and 3D printing techniques can be used to fabricate transistors.

current during the turn-on/turn-off of the gate voltage arise from the gate current being added to the drain current, due to the common source biasing configuration.<sup>[7,24]</sup> A slight non-zero  $I_G$  current is also seen at  $t < 0$  and is due to typical background Faradaic processes seen in OECTs.<sup>[25]</sup> The output characteristics of the OECT are shown in Figure 2b. A series of gate voltages from 0 to 800 mV with a step voltage of 50 mV were applied and  $I_D$  was collected as  $V_D$  was gradually varied from 0 to -1 V. A 10 s delay between sourcing voltage and measuring current was used for each voltage step to allow the device to reach a steady state timescale where transistor characteristics can be observed. Additional hysteresis sweeps are provided in Figure S4, Supporting Information. Finally, Figure 2c shows the transfer curve and the associated transconductance. A small hysteresis is observed as the gate voltage is scanned up and then down. Finally, Figure 2c shows the transfer curve and the associated transconductance. A small hysteresis is observed as the gate voltage is scanned up and then down. This can be attributed to the timescale used in the acquisition of data. Overall, these characteristics are typical for depletion mode operation, demonstrating the successful fabrication of OECTs using this hybrid FDM/inkjet printing approach to fabrication.

### 2.3. Neuromorphic Behavior

It is also found that the printed OECTs can perform neuromorphic processing functions, as shown in Figure 3. First, a paired-pulse depression (PPD) is demonstrated in Figure 3a, where two stimuli elicit different responses as the system retains the memory of the first stimulus.<sup>[7,26–31]</sup> In neuromorphic devices, this is modeled by a pair of pulses separated by a time interval  $\Delta t$ , applied here at the gate electrode. Two pulses with amplitude of 500 mV, a width of 10 s, and  $\Delta t$  was 10 s are applied at the gate under a constant  $V_D$  of -500 mV. The resultant  $I_D$  is shown to exhibit two corresponding spikes  $A_1$  and  $A_2$ , indicated with arrows in the inset of Figure 3a. During the second spike, the modulation in the current is smaller, indicating that the OECT maintains the memory of the first spike. The dependence of this memory on  $\Delta t$  is also shown in Figure 3a. As  $\Delta t$  is varied from 0.5 to 80 s, the normalized modulation in the amplitude of the second spike decreases. This is typical PPD behavior, where the memory of the first spike fades away as the interval between the two spikes increases.

The second neuromorphic processing function is that of adaptation.<sup>[28,32]</sup> Studies in visual,<sup>[33]</sup> auditory,<sup>[34]</sup> and olfactory<sup>[35]</sup> functions have shown that adaptation is an efficient

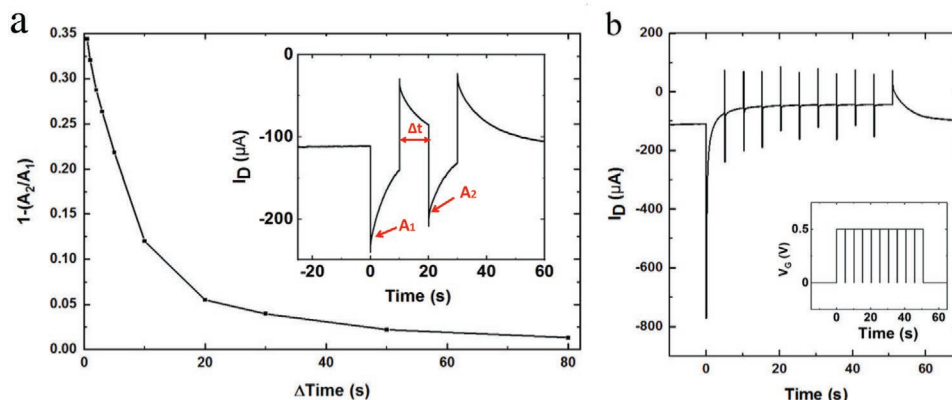


**Figure 3.** Neuromorphic properties of the printed device. a)  $I_D$  depression percentage as a function of pulse interval  $\Delta t$ . Frequency resolution can be seen in the learning characteristics of the device (insert). A pair-pulse-depression response at  $\Delta t = 10$  s. b) Adaptation in OECTs. A train of  $V_G$  pulses is applied to the device and the  $I_D$  is measured as a function of time. The device initially gives a spike timing-dependent plasticity (STDP) and subsequently adapts.

learning mechanism that tracks rapid information changes while encoding basic context.<sup>[7,10,28,32–34]</sup> A train of pulses with an amplitude of 500 mV, a width of 10 s, and separated by a time interval of 100 ms was applied to the gate electrode and Figure 3b shows the resulting adaptation in the drain current of the OECT. On application of the first pulse, the drain current changes to a new steady state, while on application of the subsequent pulses, this change decreases and eventually disappears, i.e., the current adapts to a new steady-state value. This is because injected cations have insufficient time to return to the electrolyte before a new pulse arrives. At the same time, spikes in the current during the turn-on/turn-off of the gate voltage show the device can still capture basic context in rapid information changes.

## 2.4. Discussion

The results presented above show that a hybrid of accessible and design-flexible AM techniques can be used to rapidly fabricate devices that exhibit good OECT and neuromorphic performance. One significant advantage of digitally manufactured OECTs is the fact that their performance and geometrical design can be rapidly optimized to suit a given application. For example, the response time is proportional to the volume of the semiconductor film, while the transconductance scales as  $w \times d/L$ , where  $d$  is the thickness of the semiconductor film,  $w$  is the width of the source and drain electrodes, and  $L$  is their distance.<sup>[36]</sup> In this work, we have focused entirely on large channel lengths. This results in longer electron transit times and slower transistor characteristics. We see this in the comparatively longer timescales in the transient responses of the devices reported here. This ability for rapid design change is anticipated to enable neuromorphic devices with tailored responses, which will be explored in future work as we refine channel dimensions. One limitation in the current design is the high resistivity ( $\approx 0.18 \Omega \text{ m}$ ) of the printed thermoplastic polymer, c-PLA, meaning that there is currently significant resistive loss across the source and drain

electrodes. However, the palette of materials used for FDM is rapidly expanding and recent research and commercialization activities have shown alternative 3D-printing thermoplastic filaments with lower resistivity values down to  $0.006 \Omega \text{ m}$ , by integrating metallic nanostructures or 2D conducting materials such as graphene or large carbon platelets.<sup>[37–40]</sup> Initial tests with other architectures have shown the approach to be very robust. It will, however, be critical to study further the role of printing direction, layer thickness, and alternative materials on the yield, repeatability, and long-term stability of these devices.

## 3. Conclusion

Hybrid additive manufacturing systems that combine FDM with inkjet printing are in their early stages of development, with most systems being built to enable color patterning of 3D printed structures.<sup>[41,42]</sup> The advantages of FDM/inkjet hybrid approaches have already been noted for integration of conductive paths.<sup>[43–45]</sup> Both direct-write technologies are already scalable, suitable for fabricating structures with hundreds of layers, and have well-understood formulation and filament/ink requirements.<sup>[37–40,46,47]</sup> The work here using standard materials and techniques to fabricate OECTs and to demonstrate neuromorphic behavior demonstrates a clear path for translation to more complex structures and devices that can then progress to applications in bioelectronics.<sup>[1,48]</sup>

In conclusion, we showed that a digitally enabled hybrid approach to additive manufacturing, combining FDM with inkjet printing, can be used to rapidly fabricate neuromorphic transistors with commercially available materials. The OECTs showed clear depletion-mode operation, paired-pulse depression behavior, and evidence of adaptation to support this conclusion. Given the mechanical and architectural flexibility of a hybrid FDM/inkjet printing technique, it is anticipated that this work will enable integration of bioelectronics and neuromorphic behavior into personalized, multilayer devices created by additive manufacturing.



## 4. Experimental Section

**Printing:** The device was designed using Autodesk Inventor CAD software and exported as STL files.<sup>[49,50]</sup>

FDM printing software, CURA, was used to transform the STL file into G-code that was used to print the device.<sup>[49,50]</sup> A dual extrusion Ultimaker 3 3D printer was used to deposit insulating and conducting polymer filament forming the electrodes and housing of the device. The 3D printer used AA 0.4 print cores with 2.85 mm diameter filament. The total length of the device was 35 mm. The channel length of the device was 3 mm long with a width of 10 mm. The targeted layer thickness for all the 3D printing was constant at 0.06 mm. The lateral resolution targeted was 0.35 mm. All parts were printed using 100% infill.

**Materials for 3D Printing:** For the FDM insulating components, thermoplastic co-polyester (TPC) trade named Natural FLEX 45 from RS components was used. The material was selected as it exhibits good mechanical flexibility, durability, and good resistance to chemicals. To characterize the material,  $20 \times 10 \text{ mm}^2$  of 0.06 and 0.3 mm thicknesses were printed. The samples were then sputtered with Pt to make conductive pads on both sides of the material. Measurements were then taken across the thickness of the material using the Keithley 4200A-SCS Parameter Analyzer. Measurements showed that the dielectric properties of the material were maintained up to  $\approx 50 \text{ V}$  for print thicknesses of 0.06 mm. A composite polylactide resin (PLA) incorporated with carbon black and additional black conducting compound from Proto-Pasta was used to form conducting components of the device. To characterize the material, five batches of electrodes were fabricated. Each batch had 12 electrodes covering a range of lengths ( $L$ ), widths ( $W$ ), and thicknesses ( $T$ ) and were 3D printed using the c-PLA. Two-point resistance measurements were obtained using a Keysight bench digital multimeter, with examples in Figure S5, Supporting Information. From the measurements, resistivity was calculated, using measured values of the geometry, as  $0.181 \Omega \text{ m}$  with a standard deviation of  $\pm 0.029 \Omega \text{ m}$  across all electrodes. The conductivity and mass of the printed materials was monitored with exposure to electrolyte for 21 days and no changes were observed, indicating stability over the lifetime of the experiments reported.

**Inkjet Printing:** Inkjet printing was carried out with a FUJIFILM Dimatix Materials Printer DMP-2850, using the 10 pL Fuji Film Dimatix Materials printhead. Prior to printing, to enable thin film formation across the channel, a corona treatment setup (Lab System IV, LabTec) was used with a setting of 21 kV under ambient air. Areas with exposed c-PLA were covered with masking tape to avoid damage from the plasma. During the print period, 5 or fewer nozzles were used to jet at an amplitude of 16 V and with a 15  $\mu\text{m}$  drop spacing. A print area of 6 mm  $\times$  10 mm was used to ensure coverage of the 3 mm  $\times$  10 mm channel and contact with the electrodes, and four layers were printed for the experiments detailed here. The device was then hard baked or 60 min at 130  $^{\circ}\text{C}$ .

**Materials for Inkjet Printing:** The PEDOT:PSS used was Clevios PH 1000 from Heraeus Holding GmbH and is provided as 1–1.3 wt% PEDOT:PSS dispersed in water. To make a printable ink, additions were made of 5 wt% ethylene glycol (EG), 0.1 wt% dodecyl benzene sulfonic acid (DBSA), and 1 wt% of (3-glycidyloxypropyl)trimethoxysilane (GOPS). The additives DBSA, GOPS, and EG were added to optimize ionic and electronic conductivity of the film.<sup>[20,49,50]</sup> The printed, cross-linked film was found to be stable upon submersion in the aqueous environment and was measured as  $2.15 \pm 0.23 \mu\text{m}$  in thickness, as noted in Figure S3, Supporting Information.

**Device Characterization:** PBS solution (0.01 M) was used as the electrolyte material. The solution was formed by adding a PBS pallet from Sigma-Aldrich to DI water. An Ag/AgCl electrode (World Precision Instruments) was used as a gate electrode. A Keysight B1500a semiconductor device analyzer was used for device characterization. Testing reported here was repeated on a single device ten times over the period of a month to ensure results were representative and stable. The coefficient of variation was noted in the  $I_D$  and  $I_G$  response of 9.45% and 2.0%, respectively, as obtained at  $V_D = -900 \text{ mV}$  and  $V_G = 800 \text{ mV}$ .

## Supporting Information

Supporting Information is available from the Wiley Online Library or from the author.

## Acknowledgements

This work was funded by the EPSRC Centre for Doctoral Training in Ultra Precision Engineering (EP/L016567/1). S.Y. acknowledges the support of Leading Young Researcher Overseas Visit Program from Tohoku University. The authors gratefully acknowledge the contributions from members of the Fluids in Advanced Manufacturing and the Bioelectronics Laboratory groups (Department of Engineering, University of Cambridge).

## Conflict of Interest

The authors declare no conflict of interest.

## Data Availability Statement

The data that support the findings of this study are available from the authors upon request.

## Keywords

3D printing, fused deposition modeling, inkjet printing, neuromorphic devices, organic electrochemical transistors

Received: August 12, 2020

Revised: September 30, 2020

Published online: November 13, 2020

- [1] J. Rivnay, S. Inal, A. Salleo, R. M. Owens, M. Berggren, G. G. Malliaras, *Nat. Rev. Mater.* **2018**, 3, 17086.
- [2] D. A. Bernards, G. G. Malliaras, *Adv. Funct. Mater.* **2007**, 17, 3538.
- [3] D. Khodagholy, J. Rivnay, M. Sessolo, M. Gurfinkel, P. Leleux, L. H. Jimison, E. Stavrinidou, T. Herve, S. Sanaur, R. M. Owens, G. G. Malliaras, *Nat. Commun.* **2013**, 4, 2133.
- [4] J. Rivnay, S. Inal, B. A. Collins, M. Sessolo, E. Stavrinidou, X. Strakosas, C. Tassone, D. M. Delongchamp, G. G. Malliaras, *Nat. Commun.* **2016**, 7, 11287.
- [5] J. Rivnay, R. M. Owens, G. G. Malliaras, *Chem. Mater.* **2014**, 26, 679.
- [6] C. D. Dimitrakopoulos, P. R. L. Malenfant, *Adv. Mater.* **2002**, 14, 99.
- [7] P. Gkoupidenis, N. Schaefer, B. Garlan, G. G. Malliaras, *Adv. Mater.* **2015**, 27, 7176.
- [8] E. R. W. van Doremale, P. Gkoupidenis, Y. van de Burgt, *J. Mater. Chem. C* **2019**, 7, 12754.
- [9] C. D. Schuman, T. E. Potok, R. M. Patton, J. D. Birdwell, M. E. Dean, G. S. Rose, J. S. Plank, *arXiv:1705.06963* **2017**.
- [10] L. F. Abbott, W. G. Regehr, *Nature* **2004**, 431, 796.
- [11] D. O. Hebb, *The Organization of Behavior: A Neuropsychological Theory*, Psychology Press, East Sussex, UK **2005**.
- [12] P. Gkoupidenis, S. Rezaei-Mazinani, C. M. Proctor, E. Ismailova, G. G. Malliaras, *AIP Adv.* **2016**, 6, 111307.
- [13] P. Gkoupidenis, D. A. Koutsouras, G. G. Malliaras, *Nat. Commun.* **2017**, 8, 15448.

- [14] R. A. Cirelli, G. P. Watson, O. Nalamasu, in *Encyclopedia of Materials: Science and Technology* (Eds: K. H. J. Buschow, R. W. Cahn, M. C. Flemings, B. Ilshner, E. J. Kramer, S. Mahajan, P. Veyssière), Elsevier, Oxford **2001**, pp. 6441–6448.
- [15] D. Khodagholy, V. F. Curto, K. J. Fraser, M. Gurfinkel, R. Byrne, D. Diamond, G. G. Malliaras, F. Benito-Lopez, R. M. Owens, *J. Mater. Chem.* **2012**, 22, 4440.
- [16] B. Kolodziejczyk, C. Hin Ng, X. Strakosas, G. G. Malliaras, B. Winther-Jensen, *Mater. Horiz.* **2018**, 5, 93.
- [17] S. A. Tria, L. H. Jimison, A. Hama, M. Bongo, R. M. Owens, *Biochim. Biophys. Acta, Gen. Subj.* **2013**, 1830, 4381.
- [18] H. Yuk, B. Lu, S. Lin, K. Qu, J. Xu, J. Luo, X. Zhao, *Nat. Commun.* **2020**, 11, 1604.
- [19] G. Istamboulie, T. Sikora, E. Jubete, E. Ochoteco, J.-L. Marty, T. Noguer, *Talanta* **2010**, 82, 957.
- [20] H. Yan, H. Okuzaki, *Synth. Met.* **2009**, 159, 2225.
- [21] Y. Yoshioka, G. E. Jabbour, *Synth. Met.* **2006**, 156, 779.
- [22] D. Majak, J. Fan, M. Gupta, *Sens. Actuators, B* **2019**, 286, 111.
- [23] S. Mohr, O. Khan, *Technol. Innovation Manage. Rev.* **2015**, 5, 20.
- [24] J. T. Friedlein, R. R. McLeod, J. Rivnay, *Org. Electron.* **2018**, 63, 398.
- [25] J. T. Friedlein, M. J. Donahue, S. E. Shaheen, G. G. Malliaras, R. R. McLeod, *Adv. Mater.* **2016**, 28, 8398.
- [26] H. Z. Shouval, S. S.-H. Wang, G. M. Wittenberg, *Front. Comput. Neurosci.* **2010**, 4, 3.
- [27] A. Destexhe, E. Marder, *Nature* **2004**, 431, 789.
- [28] W. G. Regehr, *Cold Spring Harbor Perspect. Biol.* **2012**, 4, a005702.
- [29] D. Swandulla, M. Hans, K. Zipser, G. J. Augustine, *Neuron* **1991**, 7, 915.
- [30] N. T. Shah, L. C. Yeung, L. N. Cooper, Y. Cai, H. Z. Shouval, *Biol. Cybern.* **2006**, 95, 113.
- [31] J. E. Zengel, K. L. Magleby, J. P. Horn, D. A. McAfee, P. J. Yarowsky, *J. Gen. Physiol.* **1980**, 76, 213.
- [32] S. Chung, X. Li, S. B. Nelson, *Neuron* **2002**, 34, 437.
- [33] D. Gilden, R. Blake, G. Hurst, *Cognit. Psychol.* **1995**, 28, 1.
- [34] S. M. Anstis, S. Saida, *J. Exp. Psychol. Hum. Percept. Perform.* **1985**, 11, 257.
- [35] T.-Y. Chen, K.-W. Yau, *Nature* **1994**, 368, 545.
- [36] D. Khodagholy, P. Leleux, M. Ferro, M. Sessolo, A. Williamson, D. A. Koutsouras, J. Rivnay, M. Ramuz, X. Strakosas, R. M. Owens, C. Benar, J.-M. Badier, C. Bernard, G. G. Malliaras, *Sci. Adv.* **2015**, 1, e1400251.
- [37] K. Gnanasekaran, T. Heijmans, S. van Bennekom, H. Woldhuis, S. Wijnia, G. de With, H. Friedrich, *Appl. Mater. Today* **2017**, 9, 21.
- [38] X. Wei, D. Li, W. Jiang, Z. Gu, X. Wang, Z. Zhang, Z. Sun, *Sci. Rep.* **2015**, 5, 11181.
- [39] P. F. Flowers, C. Reyes, S. Ye, M. J. Kim, B. J. Wiley, *Addit. Manuf.* **2017**, 18, 156.
- [40] V. B. Mohan, B. J. Krebs, D. Bhattacharyya, *Mater. Today Commun.* **2018**, 17, 554.
- [41] F. Regina, F. Lavecchia, L. M. Galantucci, *Int. J. Interact. Des. Manuf.* **2018**, 12, 979.
- [42] Y.-C. Chang, H.-T. Hsieh, EP3345741A1, **2018**.
- [43] W. Zhou, F. A. List, C. E. Duty, S. S. Babu, *Rapid Prototyp. J.* **2016**, 22, 77.
- [44] K. A. Nate, J. Hester, M. Isakov, R. Bahr, M. M. Tentzeris, in *2015 European Microwave Conf. (EuMC)*, IEEE, Piscataway, NJ **2015**, <https://ieeexplore.ieee.org/document/7345837>.
- [45] J. Bito, R. Bahr, J. Hester, J. Kimionis, A. Nauroze, W. Su, B. Tehrani, M. M. Tentzeris, *Micro-and Nanotechnology Sensors, Systems, and Applications IX*, Vol. 10194, International Society for Optics and Photonics **2017**.
- [46] I. M. Hutchings, G. D. Martin, *Inkjet Technology for Digital Fabrication*, Wiley, New York **2012**.
- [47] S. D. Hoath, *Fundamentals of Inkjet Printing: The Science of Inkjet and Droplets*, Wiley, New York **2016**.
- [48] D. Khodagholy, T. Doublet, P. Quilichini, M. Gurfinkel, P. Leleux, A. Ghestem, E. Ismailova, T. Hervé, S. Sanaur, C. Bernard, G. Malliaras, *Nat. Commun.* **2013**, 4, 1575.
- [49] Autodesk Inventor Professional, <https://www.autodesk.com/education/free-software/inventor-professional> (accessed: March 2020).
- [50] Simplify 3D printing with Ultimaker Cura 4.0, <https://ultimaker.com/learn/simplify-3d-printing-with-ultimaker-cura-4-0> (accessed: March 2020).
- [51] O. P. Dimitriev, D. A. Grinko, Y. V. Noskov, N. A. Ogurtsov, A. A. Pud, *Synth. Met.* **2009**, 159, 2237.
- [52] M. ElMahmoudy, S. Inal, A. Charrier, I. Uguz, G. G. Malliaras, S. Sanaur, *Macromol. Mater. Eng.* **2017**, 302, 1600497.